Nanoscale

Accepted Manuscript

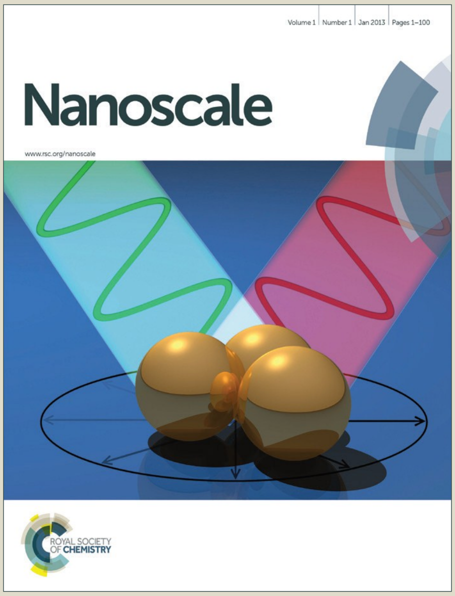

This is an *Accepted Manuscript*, which has been through the Royal Society of Chemistry peer review process and has been accepted for publication.

Accepted Manuscripts are published online shortly after acceptance, before technical editing, formatting and proof reading. Using this free service, authors can make their results available to the community, in citable form, before we publish the edited article. We will replace this *Accepted Manuscript* with the edited and formatted *Advance Article* as soon as it is available.

You can find more information about *Accepted Manuscripts* in the Information for Authors.

Please note that technical editing may introduce minor changes to the text and/or graphics, which may alter content. The journal's standard Terms & Conditions and the Ethical guidelines still apply. In no event shall the Royal Society of Chemistry be held responsible for any errors or omissions in this *Accepted Manuscript* or any consequences arising from the use of any information it contains.

ROYAL SOCIETY OF CHEMISTRY

www.rsc.org/nanoscale

A tactile sensor using a conductive graphene-sponge composite

Sungwoo Chun, Ahyoung Hong, Yeonhoi Choi, Chunho Ha, and Wanjun Park*

Department of Electronics Engineering, Hanyang University, Seoul 133-791 South Korea

Nanoscale Accepted Manuscript

Abstract

For sensors that emulate human tactile perception, we suggest a simple method for fabricating a highly sensitive force sensor using a conductive polyurethane sponge where graphene flakes are self-assembled into the porous structure of the sponge. The completed sensor device shows a sensitive and reliable response for a broad range of pressure and dynamic pressure detection that correspond to human tactile perception. The ability of the sensor to detect vibration is also confirmed with vertical actuations due to slipping over micro-scale ridge structures attached on the sensors. Based on the sensor's ability to detect both pressure and vibration, the sensor can be utilized as a flexible tactile sensor.

Keywords: Graphene sponge, Pressure sensor, Tactile sensor, Dip-coating, Porous sponge.

***Corresponding author:** E-mail: wanjun@hanyang.ac.kr , Tel: +82-2-2220-4315.

1. Introduction

Among the five senses that humans employ to interact with the environment, tactile sensing is the biological recognition of touch experienced through responses of the cutaneous mechanoreceptors reacting to pressure and vibration induced by direct contact with a material surface. Human skin shows excellent touch sensitivity through four mechanoreceptors that function as sensor elements in glabrous skin. These include Pacinian corpuscles (for rapid vibrations of 40 to 400 Hz), Meissner's corpuscles (for light touch and texture changes around 5 to 50 Hz), Merkel's discs (for sustained pressure), and Ruffini endings (for tension deep in the skin) [1]. To emulate such functions, an artificial sensor basically requires high sensitivity in the pressure range corresponding to human pressure perception (100 to 100,000 Pa) and sensitive detection of vibrations up to ~400 Hz to recognize the texture information of touched materials [2].

Flexible force sensors are regarded as detecting elements for tactile sensation because the sensor operation can be performed on soft substances. Some demonstrations of such sensors have been reported with the development of conductive polymers [3-6] or the introduction of various nano-materials (including nanowires, nanotubes and graphene) into soft substrates [7-13]. However, research efforts are mainly focused on enhancing the sensitivity of pressure detection and detection of pressure distributions. Recognition of vibrations using force sensors has largely been ignored, although it would be ideal if a force sensor could be applied for detection of both pressure and vibration.

In this work, we present a highly sensitive sensor using graphene-sponge composites (GSCs), which can emulate human tactile sensation by recognizing both pressure and vibration in the human sensing range with a single element architecture. To achieve a piezo-resistive substance, conductive graphene flakes (GFs) are introduced into a polyurethane

Nanoscale Accepted Manuscript

sponge (PS) as a soft substrate to achieve both electrical conductivity and mechanical flexibility. The porous structure of the sponge provides an advantage in improving the response for vibration detection in addition to providing high sensitivity to the applied pressure. Such properties allow the sensor to distinguish the surface texture of materials during a touching event.

2. Formation of conductive graphene-sponge composite

Formation of a template-assisted sponge structure with graphene has been studied with various methods, which are categorized by direct growth on a porous catalytic metal [14-17] or coating of a porous template using graphene dispersed in an aqueous solution [18-21]. Among these methods, the dip coating method with conductive graphene flakes (GFs) is employed for fabrication of the conductive graphene-sponge composite (GSC) in this work because the process is simple and practical [22]. The commercially available PS is directly immersed in a GF solution for 3 hours followed by drying to yield a robust form where the GFs are firmly stuck in the internal skeletons of the PS as shown in **Fig. 1**a. As displayed in **Fig. 1**b, the GFs are coated along the skeletons of the PS (**Fig. 1**c) and were embedded as aggregated particles into vacancies of the porous structure (**Fig. 1**d). The aggregated GF particles filled the vacancies of the porous PS structure. It is noted that graphene insertion in polyurethane nanofiber induces slight enhancement of elastic characteristics which are resulting fast recovery time for shape deformation [23]. PS is also expected for the similar behavior in elastic character with GF insertion. The GF particles are critical for providing piezo-resistive character because the number of contacts between the particles increases with increasing force, which results in an increase in conductive paths. The dip-coating method generally employs graphene oxide flakes (GOFs), which require an oxidation-reduction

Nanoscale Accepted Manuscript

process because oxidized graphene provides a uniform coating on the surface of the template by preventing aggregation of graphene flakes in solution [24-26]. Conductive paths are only formed along the skeleton of the sponge, and force sensor applications require additional modification for enhancement of conductivity and piezo-resistive character as demonstrated in previous work [27]. On the other hand, the GFs easily aggregate upon dispersion in water because of their hydrophobic character. By applying the GFs instead of GOFs, the resulting GF particles increase the conducting paths of the GSC that can enhance piezo-resistive characteristics. Therefore, the incorporation of GFs must be customized to produce a conductive GSC that can function as a piezo-resistive substance.

The GFs and aggregated GF particles are uniformly and firmly coated on the entire surface of the PS skeletons that make up the structure of the sponge. This uniform coating makes the GSC hydrophobic due to the surface character of graphene. **Fig. 2**a shows a comparison of the water affinity between the sponge and the GSC. As shown, the sponge sinks into water, but the GSC floats on the water surface. **Fig. 2**b also confirms the water resistance due to the clear formation of water droplets on the GSC, while water droplets are easily absorbed into the sponge. Typical Raman resonance peaks (Supplemental information Figure S1) for the coated layered graphene are observed for a randomly selected area on the GSC. In addition, the embedded GFs maintain their attachment without any specific process to affix. The adhesion strengths due to Van der Waals interaction [28-29] are high because the surface tensions of graphene to graphene and graphene to internal polyurethane surface are strong enough to withstand the mechanical stresses induced by twisting (**Fig. 2**c) and hitting (**Fig. 2**d) (Supplemental video clips: SV1 and SV2). **Fig. 2**e shows that the resistances of the GSC were maintained against twisting and hitting stresses after a few initial applications, which also implies uniform and robust attachment of GFs.

Nanoscale Accepted Manuscript

The advantage of using the dip-coating method with a GF dipping solution is that the conductivity of the GSCs can be easily adjusted by changing either the GF concentration in the dispersion solution or the number dips. **Fig. 3**a shows the results of two GSCs, which are treated with three (left) and thirty (right) dipping repetitions, respectively, in a 1 mg/ml graphene dispersion. The sponge is initially white, but becomes darker with increased dipping repetitions due to deposition of the GFs. As displayed in **Fig. 3**b, the cut surfaces at the middle of the sponges also show uniform and equivalent darkness corresponding to each dipped sponge. This indicates that the absorbing ability of the sponge is strong enough to form a continuous coating of GFs inside the sponge. **Fig. 3**c shows that the electrical conductivity depends on the dipping process, which depends on the GF concentration in the dispersion solution and the number of dips. The conductivity tends to increase up to a saturation value of 5.24 mS/cm with a GF concentration of 2 mg/ml after 30 dips, while larger GF concentrations than 0.25 mg/ml are required to obtain conductive GSCs in a single dip.

Nanoscale Accepted Manuscript

3. Force sensor using conductive graphene-sponge composite

The elastic character of the sponge allows the GSCs to be used in force sensor applications. As shown in **Fig. 4**a, the applied force enhances connections between the aggregated GFs coated on the skeletons of the internal porous structure of the sponge. The force sensor is completed by adding Pt electrodes protected by PEN (polyethylene naphthalate) films on the top and bottom sides of the GSC (1.5 x 1.5 x 1.5 cm^3). **Fig. 4**b shows the change in conductance ($\Delta C = C - C_0$) for the selected applied pressures (0.24, 1, 10 kPa) relative to the initial conductance of the sensor C_0 (3.08 mS) before applying the force. For this sensor, a GSC with a conductivity of 2.05 mS/cm was fabricated by 30 dipping repetitions in the GF solution (1 mg/ml). The increases in the conductance (ΔC) are attributed to a decrease in the spatial vacancies in the GSC as a function of the applied pressure. All measurements are performed in a home-made apparatus equipped with a time controlled force inductor. Reproducible operation is also confirmed through 2,000 repeated 2,000 loading-unloading cycles with a pulse width of 2 Hz and a pressure of 2 kPa (Supplemental information Figure S2). **Fig. 4**c shows $\Delta C/C_0$ for a vertical pressure input of 13 to 20,000 Pa. The pressures are applied by stacking weights with surface areas that are identical to that of the sensor. We generally defined sensitivity as $S= (\Delta C/C_0)/\Delta P$, and two different slopes are estimated from rough linear fits as 1.04 kPa^{-1} for the applied pressure regions of 13 to 260 Pa and 0.12 kPa^{-1} for 260 to 20,000 Pa. The increase in the conductivity gradually saturates with increasing pressure because the effective vacancies are reduced by the force. The sensitivity varies with GSC thickness as thinner GSC shows higher sensitivity (Supplemental information Figure S3).

Fig. 5a shows the dynamic responses for the vertical pressure applied as a time-dependent pulse. Measurements are carried out using a homemade apparatus, which includes a source meter and a pressure inductor that supplies the dynamic vertical forces. The output conductance change ratio ($\Delta C/C_0$) is consistently measured as ~0.52 for each applied pressure (1 kPa) with a 0.5 s pulse width and duration, and 0.2 s measurement intervals. **Fig. 5**b displays the same measurement performed with a 0.2 s pulse width and duration, and 0.2 s measurement intervals that indicate simultaneous responses for the applied pressure. $\Delta C/C_0$ is consistently measured as 60 for 640 kPa, which is the maximum limit of the force inductor (Supplemental information Figure S4). As shown in **Fig. 5**c, the response time for the sensor is estimated to be as fast as ~ 34 ms for deformation by an applied pressure of 500 Pa and 5 ms for restoration due to the self-recovery of the elastic character of the GSC with 0.1 ms

Nanoscale Accepted Manuscript

measurement intervals. The deformation time could be overestimated because of limitations in the delay accuracy (10 ms) of the pressure inductor in the measurement apparatus. Apart from the high sensitivity and fast response, the advantage in using an elastic sponge is that it allows for detection of infinitesimal pressures. **Fig. 5**d shows responses of the sensors for a 2.3 Pa applied pressure driven by a weight of 110.7 mg with an area of 4.84 cm^2.

4. Detection of surface roughness for tactile sensing

The vibration detection is another required function for emulating tactile sensing beyond simple force measurements. The observed sensor characteristics actually mimic human perception even described by fast adapting (FA) mechanoreceptors (Pacinian and Meissner) that are detecting vibrations at frequencies up to 400 Hz [1]. **Fig. 6** shows the frequency responses for the sensor in various vibration ranges (1 to 500 Hz). For a vertically applied vibration induced by an actuator driven using a function generator, the frequency responses are read using an oscilloscope to estimate the signal to noise ratio (SNR). The sensor has a good SNR (as defined as the output voltage difference) over 20 dB up to a frequency of 50 Hz; then, the signals gradually decrease with increasing frequency. This degradation is attributed to an incomplete sensor response due to the time lag resulting from elastic deformation and restoration of the sponge. In spite of such degradation, the SNR does not drop below 10 dB up to 500 Hz.

The high sensitivity of the sensor (especially in the extremely low pressure region) allows for detection of a locally applied force by a partial segment on the sensor as displayed in **Fig. 7**a. This figure shows a schematic of the shear force measurement by using a flexible ridge (height x width = 80 x 200 μm) introduced on the sensor. The ridge structure is fabricated using polyethylene terephthalate (PET) because it is flexible and compatible with

Nanoscale Accepted Manuscript

conventional lithography and etching processes. The slip motion of the PET tip (width = 120 μm) generates an interacting force through a touching event between the tip and the ridge. The force is transferred to the local area of the GSC, defined by the ridge width and length.

Fig. 7b shows the output conductance change ratio for the transferred local force with a slip velocity of 1 mm/s directed forward and backward for a sensor equipped with single and double ridges. A five percent conductance change is equivalent to the case where 40 Pa is uniformly applied to the entire area of the sensor. The corresponding force is estimated to be 9 mN for a sensor area of 2.25 cm^2. The ridge structure not only amplifies the pressure of the applied force by reducing the interacting area, but it also induces a local vibration by acting as a moving probe tip. The observed 0.3 s period in the peak width with a slip speed of $v = 1$ mm/s confirms that the interaction time over the moving distance should be defined as the sum of the ridge and tip width (320 μm). In the case of two ridges separated by 200 μm, the sensor is able to distinguish each ridge pattern without a mixture of the two peaks. The spatial resolution of the sensor for the locally applied pressure is estimated to be 80 μm by considering that the width of the tip is 120 μm. **Fig.** 7c demonstrates the frequency response after the fast Fourier transform (FFT) of the data. This response is based on the conductance output of the sensor on which the periodic ridge pattern with 200 μm separation is attached (see inset). The sensor output is also periodic because it is generated through the vibrations caused by touching events on each ridge with the constantly moving probe tip. The sensor response for such vibrations was observed as a peak in the FFT wave form whose position corresponds to the contact interaction time. The peak positions for the first harmonic are observed at 21, 32, 56 Hz for slip speeds (v) of 4, 6, and 11 mm/s respectively, with a periodic space of $v/f = 200$ μm for the ridges.

The demonstrated characteristics of the GSC sensor suggest that it can be used to emulate

Nanoscale Accepted Manuscript

tactile sensation for recognizing vibrations due to surface roughness. This is the basic function of perceiving surface texture. Generally, texture recognition using a force sensor requires a matrix architecture whose sensor elements should be integrated with a distribution density according to the required spatial resolution. However, the construction of a matrix architecture using resistive elements causes many practical difficulties involving wiring, sneaker paths, a complex driving circuit, addressing, and so on. In contrast, the demonstrated GSC sensor can be constructed to function in a single sensor architecture with the specific responsibility of detecting vibrations due to interactions generated by the pressure applied to a local area through a micro-patterned ridge structure that acts as a human finger print.

5. Conclusion

In summary, we propose a flexible tactile sensor using self-assembled conductive networks of GFs formed in a polyurethane sponge. Direct dipping of the sponge in a solution of conductive GF results in robust adherence of the GFs inside the sponge to provide a mechanically stable GSC. The extraordinary elastic properties of the sponge allow the GSC to be used as a force detecting element for sensors. The sensors fabricated using these materials provide high sensitivity over a broad pressure range and fast response for vibrations that corresponding to human perception of tactile sense. In particular, the sensor provides detection of vibrations driven from partial segments on the sensor. It also allows for surface texture recognition with a single sensor by introducing a micro-patterned ridge structure that acts as a human finger print. Based on the characteristics demonstrated in this work, the GSC sensor is a promising element for a tactile recognition system emulating human sense within a single element architecture, which is the simplest way of resolving the issues related to sensor integration.

Nanoscale Accepted Manuscript

6. Experimental

Fabrication of conductive graphene-polyurethane sponge composite

Graphene nano-powder (Graphene Supermarket Co.) with individual flake thicknesses of < ~3 monolayers, a lateral flake size of ~10 μm and a surface area of 510 m^2/g is vigorously mixed to form suspensions in dimethylformamide (DMF). Sonication is then applied by using a sonication bath for 3 hours in order to obtain mixed graphene. The mixture was then stirred with a magnetic bar (1 hour at 400 rpm). The graphene suspension is coated on the porous structure of the polyurethane sponge by the dip-coating method. Drying is conducted in a baking oven at 170°C for 2 hours and at 85°C for 24 hours. Repetitions of the dip-coating and drying process are performed to ensure an appropriate conductivity.

Sensor fabrication

Preparation of the sensors is completed with the attachment of Pt electrodes on a 50 μm thick polyethylene naphthalate (PEN) film that acted as both a substrate for evaporation and a protection layer. For tactile sensing devices, the ridge structures are prepared with polyethylene terephthalate (PET) because it is easy to fabricate and is relatively rigid. The SiO_2 layer is deposited on the PET film using plasma enhanced chemical vapor deposition at 80°C. SU-8 photo-resist is spin-coated (3000 rpm) on the SiO_2 layer followed by a two-step curing process (65°C for 3 min. and 95°C for 9 min.). Conventional optical lithography is conducted to form the ridge patterns with a height of 75 μm. The ridge patterns are completed with conventional reactive ion etching (30 sccm of CH_4 gas and 150 W of plasma power) to provide a periodic structure with a line width, height, and separation of 200, 80, and 400 μm, respectively. The tactile sensor is completed by attachment of the ridge structure on the top of the GSC with appropriate alignment.

Measurement of electrical responses of sensors

Nanoscale Accepted Manuscript

The piezoresistive responses of the sensors are independently measured through a weight stacking method using an apparatus equipped with a force inductor. In the weight stacking method, we applied weights directly on the sensor to obtain an accurate evaluation of the static pressure. The measurement apparatus devised for dynamic response of the sensor has a z-axis stage equipped with a force inductor for generating a time controlled applied pressure, a moving x-stage for slip motion, and a NI precision system SMU (PXIe-4139) connected to a Keithley 2400 sourcemeter to collect electrical data.

Measurement of surface roughness

The PET tip (width = 120 μm) slips on the PET ridge attached on the sensor with a steady velocity. Then, shear strain by physical interaction between the tip and the ridge directly generates vibrations due to interacting vertical pressures. The pressure enhances physical connections between the GFs, thus vibrations are transferred to changes of electrical conductance of the sensor. Occurrence frequency of the electrical changes is only dependent on the number of ridges, and the surface roughness is perceived after fast Fourier transform (FFT) by the function: $f = v/\lambda$, where f is vibration frequency, v is slip velocity, and λ is periodicity of ridge.

Nanoscale Accepted Manuscript

Acknowledgement

This research was supported by the NRF of Korea (2012M3A7B4035195).

References

1. R. S. Johansson, J. R. Flanagan, *Nat. Rev. Neurosci*., 2009, **10**, 345.
2. S. C. B. Mannsfeld, B. C- K. Tee, R. M. Stoltenberg, V. H-H. Christopher, S. Barman, B. V. O. Muir, A. N. Sokolov, C. Reese, Z. Bao, *Nat. Mater*., 2010, **9**, 859.
3. Q. Shao, Z. Niu, M. Hirtz, L. Jiang, Y. Liu, Z. Wang, X. Chen, *Small,* 2014, **10**, 1466.
4. L. Pan, A. Chortos, G. Yu, Y. Wang, S. Isaacson, R. Allen, Y. Shi, R. Dauskardt, Z. Bao, *Nat. Communi*., 2014, **5**, 3002.
5. C.-L. Choong, M.-B. Shim, B.-S. Lee, S. Jeon, D.-S. Ko, T.-H. Kang, J. Bae, S. H. Lee, K.-E. Byun, J. Im, Y. J. Jeong, C. E. Park, J.-J. Park, U.-I. Chung, *Adv. Mat*., 2014, **26**, 3451.
6. M. Yoonessi, Y. Shi, D. A. Scheiman, M. Lebron-Colon, D. M. Tigelaar, R. A. Weiss, and M. A. Meador, *ACS nano*, 2012, **6**, 7644.
7. S. Gong, W. Schwalb, Y. Wang, Y. Chen, Y. Tang, J. Si, B. Shirinzadeh, W. Cheng, *Nat. Communi*., 2014, **5**, 3132.
8. J. Park, Y. Lee, J. Hong, Y. Lee, M. Ha, Y. Jung, H. Lim, S. Y. Kim, H. Ko, *ACS nano,* 2014, **8**, 12020.
9. S. Chun, Y. Kim, H. Jin, E. Choi, S.-B. Lee, W. Park, *Carbon,* 2014, **78**, 601.
10. S. Chun, Y. Kim, H. Jung, W. Park, *Appl. Phys. Lett*., 2014, **105**, 041907.
11. S. Chun, H. Jung, Y. Choi, G. Bae, J. P. Kil, W. Park, *Carbon,* 2015, **94**, 982.
12. S. Chun, Y. Kim, H.-S. Oh, G. Bae, W. Park, *Nanoscale,* 2015, **7**, 11652.
13. E. Chio, O. Sul, S. Hwang, J. Cho, H. Chun, H. Kim, and S.-B. Lee, *Nanotechnology*, 2014, **25**, 425504.
14. Z. Chen, W. Ren, L. Gao, B. Liu, S. Pei, H.-M. Cheng, *Nat. Mater*., 2011, **10**, 424.
15. F. Yavari, Z. Chen, A. V. Thomas, W. Ren, H.-M. Cheng, N. Koratkar, *Sci. Rep*., 2011, **1**, 166.
16. X. Cao, Y. Shi, W. Shi, G. Lu, X. Huang, Q. Yan, Q. Zhang, H. Zhang, *Small*, 2011, **7**, 3136.
17. V. Chabot, D. Higgins, A. Yu, X. Xiao, Z. Chen, and J. Zhang, *Energy Environ. Sci*., 2014, **7**, 1564.
18. C. Wu, X. Huang, X. Wu, R. Qian, P. Jiang, *Adv. Mat*., 2013, **25**, 5658.
19. Y. Liu, J. Ma, T. Wu, X. Wang, G. Huang, Y. Liu, H. Qiu, Y. Li, W. Wang, J. Gao, *ACS Appl. Mater. Interfaces,* 2013, **5**, 10018.
20. Y. Gao, Y. S. Zhou, W. Xiong, M. Wang, L. Fan, H. Rabiee-Golgir, L. Jiang, W. Hou, X. Huang, L. Jiang, J.-F. Silvain, Y. F. Lu, *Appl. Mater. Interfaces,* 2014, **6**, 5924.
21. D. D. Nguyen, N.-H. Tai, S.-B. Lee, W.-S. Kuo, *Energy Environ. Sci*., 2012, **5**, 7908.
22. C. S. Boland, U. Khan, C. Backes, A. O'Neill, J. McCauley, S. Duane, R. Shanker, Y. Liu, L. Jurewicz, A. B. Dalton, and J. N. Coleman, *ACS nano*, 2014, **8**, 8819.
23. H. J. Yoo, S. S. Mahapatra, and J. W. Cho, *J. Phys. Chem. C*, 2014, **118**, 10408.
24. V. Chabot, D. Higgins, A. Yu, X. Xiao, Z. Chen, J. Zhang, *Energy Environ. Sci*., 2014, **7**, 1564.
25. H.-D. Liu, Z.-Y. Liu, M.-B. Yang, Q. He, *J. Appl. Polym. Sci.* 2013, **130**, 3530.
26. F. Li, X. Jiang, J. Zhao, S. Zhang, *Nano energy*, 2015, **16**, 488.
27. H.-B. Yao, J. Ge, C.-F. Wang, X. Wang, W. Hu, Z.-J. Zheng, Y. Ni, S.-H. Yu, *Adv. Mat*., 2013, **25**, 6692.
28. L. Hu, M. Pasta, F. L. Mantia, L. F. Cui, S. Jeong. H. D. Deshazer, J. W. Choi, S. M. Han, Y. Cui, *Nano Lett*., 2010, **10**, 708.
29. W. Chen, R. B. Rakhi, L. Hu, X. Xie, Y. Cui, H. N. Alshareef, *Nano Lett*., 2011, **11**, 5165.

Nanoscale Accepted Manuscript

Figure captions

Fig. 1. SEM images for (a) skeletons of pristine polyurethane sponge, (b) the GSC inside after 30 dipping repetitions in a GF solution (1 mg/ml). (c) GF coated on the skeletons of the PS, and (d) GF aggregated as particles, which partially filled the vacancies of the porous structure of the PS.

Fig. 2. (a) The pristine PS sinks under water, whereas the GSC floats on the water surface due to the hydrophobic GF coating. (b) Difference between water resistance with water droplets between the pristine PS and the GSC. Applied mechanical stresses by (c) twisting or (d) hitting to evaluate the robustness of the GSCs. (e) Electrical resistance after repeated twisting and hitting up to a thousand times for independent samples. The resistance was stably maintained regardless of the method of applying stress.

Fig. 3. Electrical conductivity of the GSCs. (a) Photographic image of two GSCs treated with three (left) and thirty (right) dipping repetitions in a solution with a GF concentration of 1 mg/ml. Inset shows the pristine PS. (b) Photographic image for cut surfaces at the middle of the GSCs. (c) Electrical conductivity as a function of the GF concentrations in the dispersion solution and number of repeated dips. The dotted line indicates conductivity of the GF film as the reference for the highest limit (0.56 S/cm).

Fig. 4. Sensor responses for applied pressure induced by static vertical forces. (a) SEM images for the aggregated GF particles filled inside the PS without and with application of vertical pressure. (b) Sensor responses in conductance change for sequential loading of applied pressure. Conductance changes are 0.27, 0.52, and 2.03 for applied pressures of 0.24, 1, and 10 kPa, respectively. (c) Sensitivity for vertical pressure of 13 to 20,000 Pa. Inset shows magnification for the low pressure regime (13 to 260 Pa).

Fig. 5. Dynamic responses for the vertical pressure applied as a time-dependent pulse. Conductance change ratio for the applied pressure (1 kPa) with a pulse width and duration of (a) 0.5 s and (b) 0.2 s. Measurement interval is 0.2 s for each case. (c) Sensor response/relaxation time for 0.1 ms of measurement accuracy with a constant bias of 10 mA. 500 Pa is applied for evaluation. (d) Sensor response for loading/unloading of 110.7 mg, which corresponds to 2.3 Pa, resulting in a conductance change ratio of 0.003.

Fig. 6. Detection of vertical vibrations. Signal to noise ratio (SNR) for the various vibration ranges (1 to 500 Hz) induced by an actuator connected to a function generator. Inset shows schematic for the vibration measurement. The red dashed line indicates a base line of 10 dB.

Fig. 7. Detection of surface roughness. (a) Description for force transfer to ridge pattern from interacting surface. The slip motion of the PET tip (width = 120 μm) generates an interacting force through a touching event between the tip and the ridge. (b) Conductance change ratio for the transferred force with a slip velocity of 1 mm/s directed forward and backward for the sensor equipped with single and double ridges. Arrows indicate the direction of the slipping motion. SEM images show the ridge structures, and each scale bar indicates 200 μm. (c) Frequency responses for the interacting vibration on the ridges during slipping motion with different slipping velocities (4~11 mm/s). The inset shows a SEM image of the periodic ridges, and the scale bar is 600 μm.

Nanoscale Accepted Manuscript

Figures

Fig. 1.

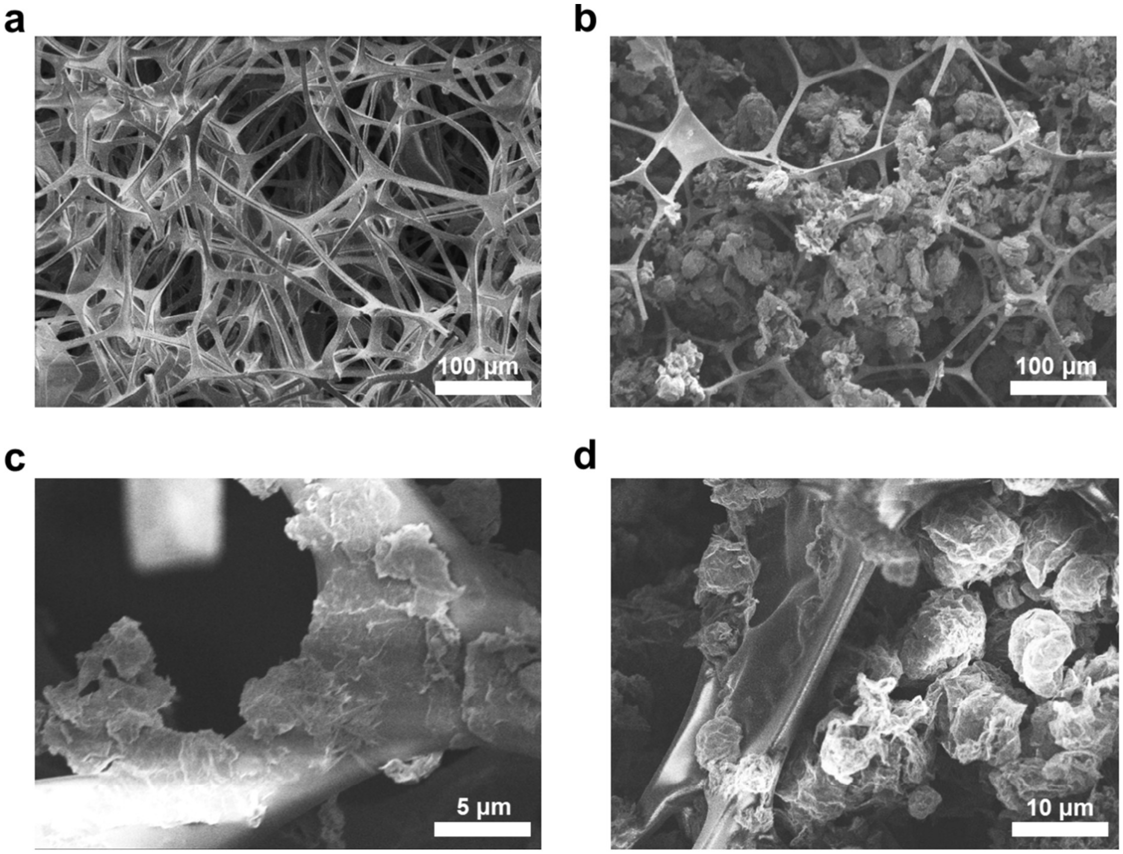

Nanoscale Accepted Manuscript

Fig. 2.

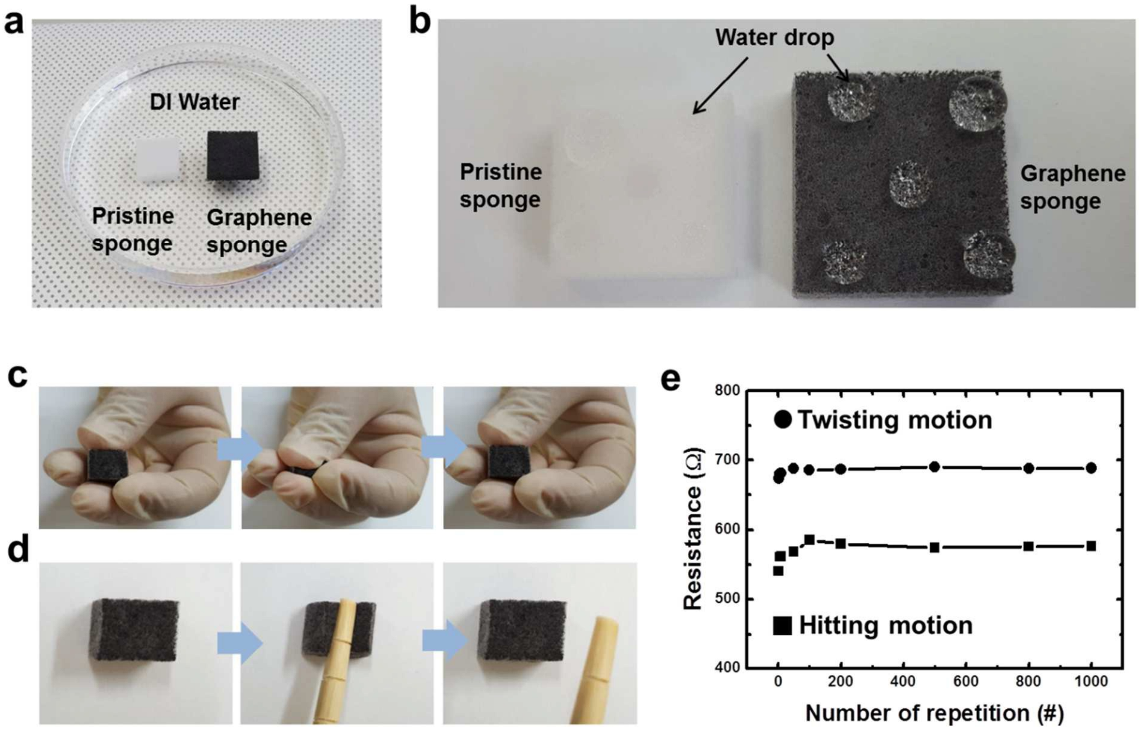

Nanoscale Accepted Manuscript

Fig. 3.

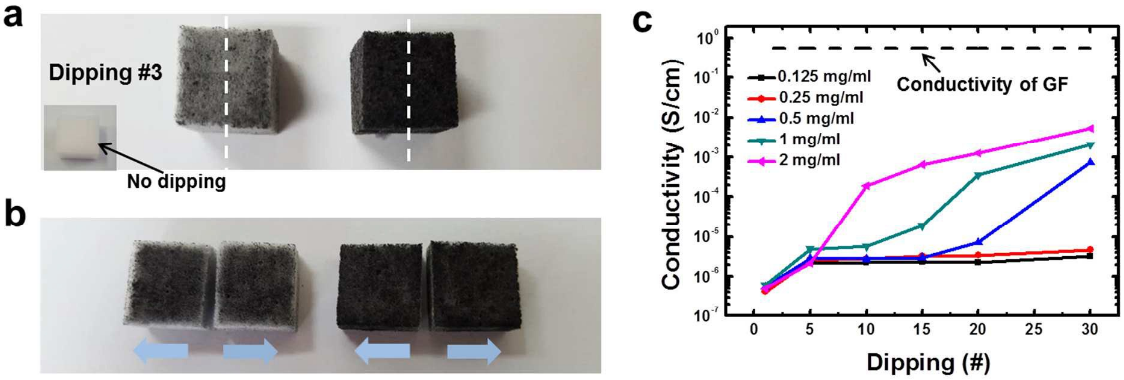

Fig. 4.

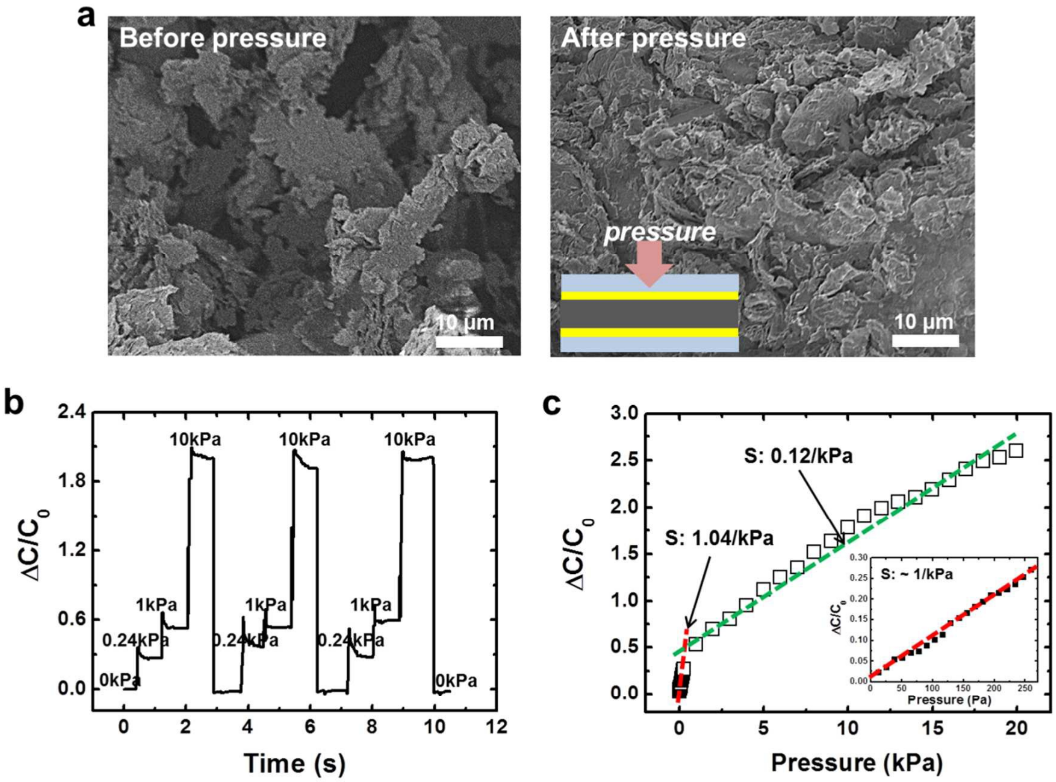

Nanoscale Accepted Manuscript

Fig. 5.

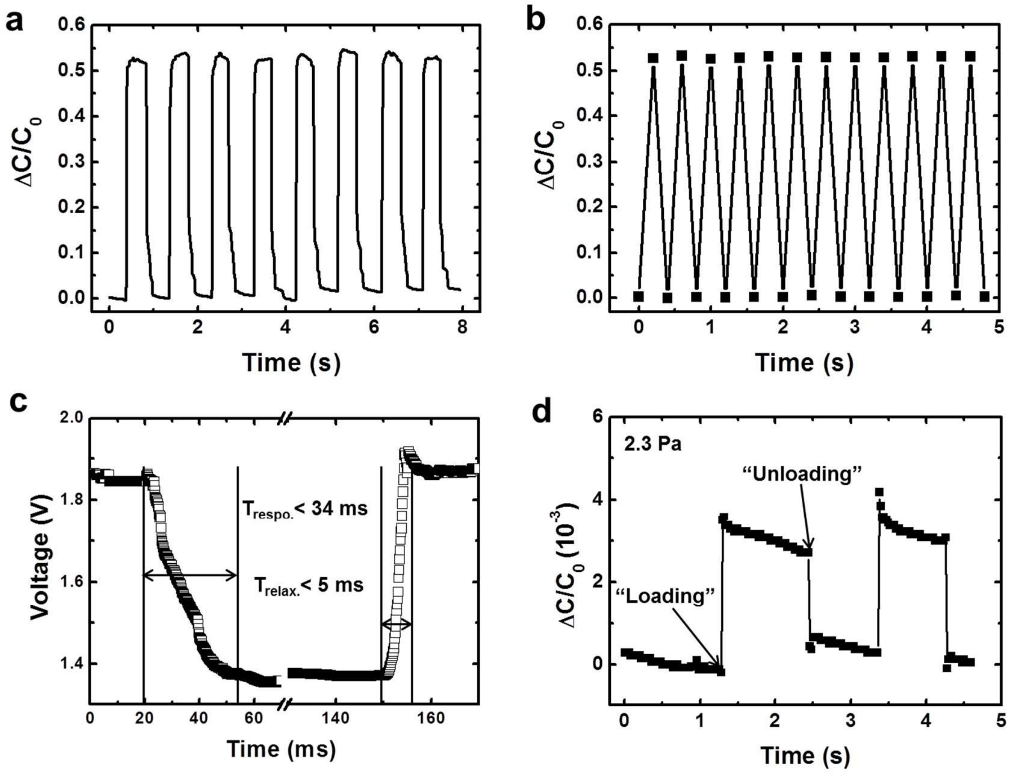

Nanoscale Accepted Manuscript

Fig. 6

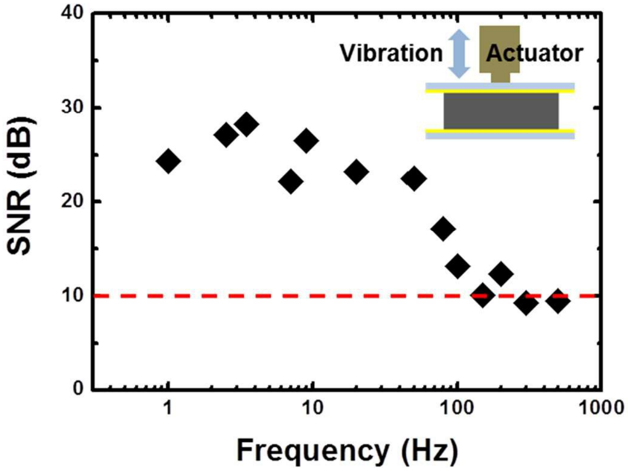

Fig. 7

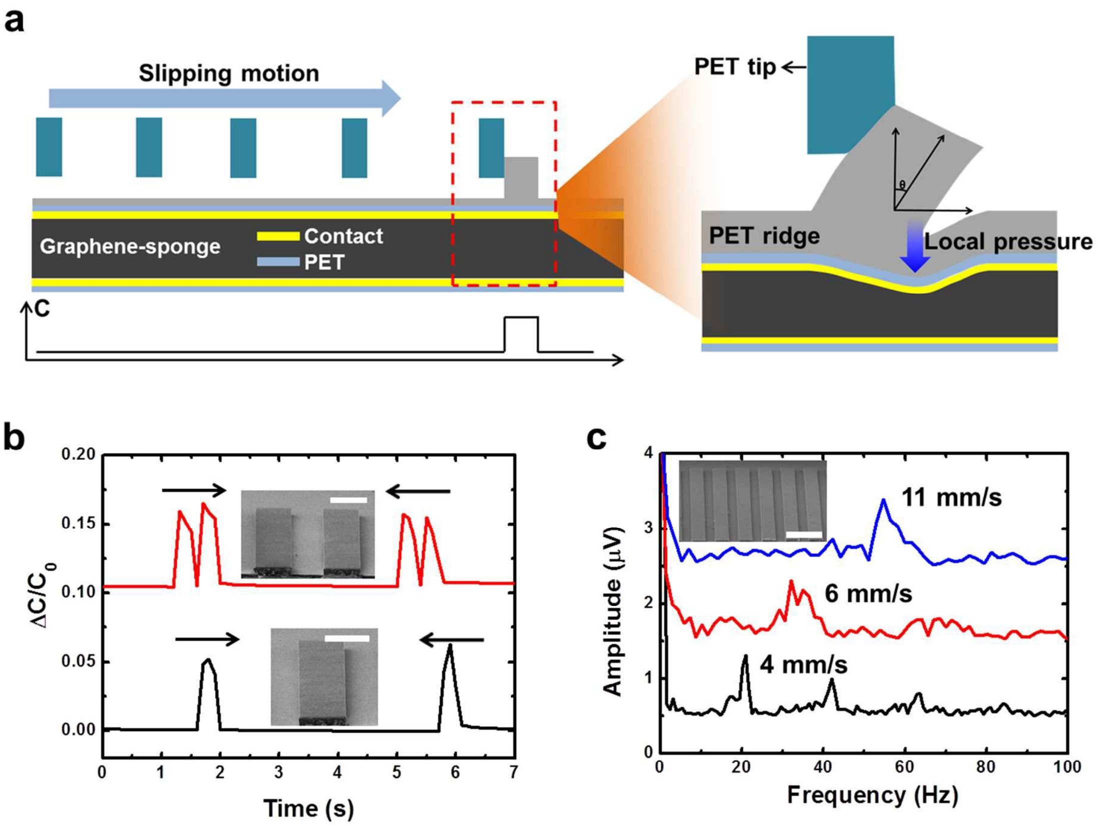

Nanoscale Accepted Manuscript